Hindawi
Advances in Materials Science and Engineering
Volume 2023, Article ID 6377399, 11 pages
https://doi.org/10.1155/2023/6377399

Research Article

The Effect of Aligned and Random PCL-Human Amniotic Membrane Powder Scaffolds on Retinal Tissue Engineering

Elahe Majidnia,[1] **Noushin Amirpour**,[2] **Mehdi Ahmadian**,[1] **Fereshteh Karamali**,[3] **and Hossein Salehi**[2]

[1]*Department of Materials Engineering, Isfahan University of Technology, Isfahan 84156-83111, Iran*
[2]*Department of Anatomical Sciences, School of Medicine, Isfahan University of Medical Sciences, Isfahan 81746-73461, Iran*
[3]*Department of Animal Biotechnology, Cell Science Research Center, Royan Institute for Biotechnology, ACECR, Isfahan, Iran*

Correspondence should be addressed to Hossein Salehi; ho_salehi@med.mui.ac.ir

Received 9 July 2022; Revised 28 October 2022; Accepted 21 November 2022; Published 3 January 2023

Academic Editor: Alicia E. Ares

One promising treatment for degenerative retinal diseases such as age-related macular degeneration (AMD) is the delivery of retinal pigment epithelial (RPE) cells using degradable scaffolds. Tough-aligned scaffolds are promising candidates for some applications of tissue engineering, such as peripheral nerve regeneration. However, aligned scaffolds have not been investigated in retinal tissue engineering so far. Here, a comparison was made between aligned and random scaffolds fabricated from polycaprolactone (PCL) and human amniotic membrane powder (HAMP) as a scaffold for RPE cells. The effects of alignment on mechanical properties, porosity, hydrophilicity, degradation of the scaffolds, and the cellular interaction of RPE cells were investigated. The results revealed that the aligned scaffold has a lower average fiber diameter, porosity, hydrophilicity, and Young's modulus and also a higher maximum strain in failure compared with the random scaffold. However, the proliferation of RPE cells increased on the random scaffold compared to the aligned scaffold. Hence, the rest of the specialized cellular evaluations, such as immunohistochemistry, real-time PCR, and functional assessments were performed on random scaffolds. The seeded cells showed an expression of RPE signature genes and functionally secreted VEGF and PEDF. Therefore, a HAMP-based substrate was fabricated for potential use as a scaffold for RPE cell transplantation.

1. Introduction

The retinal pigment epithelium (RPE), which is located between the neuroretina and the choroids, is a monolayer of pigmented cells [1]. The RPE cells interact with photoreceptor outer segments, causing the transfer of ions, nutrients, fluids, and metabolites, the polar secretion of cytokines, and the homeostasis between the photoreceptor and the choroid [2]. In degenerative retinal diseases, RPE cells lose their function, leading to the death of neural retinal cells and eventually blindness. For a long time, RPE cell transplantation has been under investigation as a treatment for these diseases. There have been many promising early results with free cell therapies; however, there are many challenges to such therapies. These challenges include the inability of free cells to attach and form a native structure, the migration of transplanted cells, and inflammation. These challenges have led researchers to tissue engineering solutions, especially scaffold-based methods [3]. Scaffolds were used to support the cells to regenerate the extracellular matrix (ECM). A suitable scaffold should be biocompatible and biodegradable, with physical and mechanical properties similar to those of native tissue for better simulation [4, 5]. Various scaffolds have been used for retinal pigment epithelial cells; however, the long-term viability and function of cells are still largely unknown [6]. Electrospun nanofibers imitate the morphology of native extracellular matrix fibers, making nanofiber scaffolds ideal for cell culture and tissue engineering applications [7].

PCL is a nontoxic, biodegradable polymer with good mechanical properties. However, its low hydrophilicity together with a lack of functional groups often results in low

cell adhesion and proliferation on these scaffolds [8–10]. The amniotic membrane (AM), the inner membrane enwrapping the fetus in the amniotic cavity [11], is considered an important potential source for the material of scaffolds. The extracellular matrix components of the basement membrane of the amniotic membrane include collagen, fibronectin, laminin, and other proteoglycans that are important for cell growth. These components are ligands for integrin receptors and therefore play an important role in cell adhesion. Other properties of the amniotic membrane include anti-inflammation, antifibrosis, antiscaring, antimicrobial, and low immunogenicity, which are all important for use in tissue engineering [12]. A combination of the PCL properties with the unique features of the amniotic membrane can result in a promising material for tissue engineering applications. Our study aimed to produce a biocompatible scaffold supporting the proliferation of RPE cells (ARPE-19 line) that could be used for the treatment of degenerative retinal diseases. In this research, two types of scaffolds with random and aligned arrangements were investigated and compared in terms of their physical and chemical properties and also for the first time in terms of the behavior of retinal pigment epithelium cells on them.

2. Materials and Methods

2.1. Materials. PCL (MW of 80000 g/mol) obtained from Sigma–Aldrich Co. was used for this study (St. Louis, MO). Formic acid (FA) and acetic acid (AA) were purchased from Merck Co. (Darmstadt, Germany), and were used as received without further purification or modification. Human placentas were taken from the cesarean section of Milad Hospital (Isfahan, Iran). ARPE-19 cells were purchased from the Isfahan Royan Institute, Iran. Dulbecco's Modified Eagle Medium (DMEM (+) Glutamax. High glucose), fetal bovine serum (FBS), trypsin/EDTA, phosphate-buffered saline (PBS), penicillin-streptomycin, and MTT (3-(4, 5-Dimethyl-2-thiazolyl)-2, 5-diphenyl-2H-tetrazolium bromide), all purchased from Bio-Idea, Tehran, Iran, were also used. QIAzol Lysis Reagent, RevertAid First Strand cDNA Synthesis, and RealQ Plus Master Mix Green high ROX™, obtained from Qiagen (America), Thermo Scientific (America), and Amplicon (Denmark), respectively, were used in the real-time PCR test. For fixing the cells before analyzing samples under the microscope, glutaraldehyde, and paraformaldehyde (Sigma–Aldrich) were used.

2.2. Electrospinning of Random and Aligned PCL-HAMP Fibrous Membranes. The electrospinning solution was prepared similarly to the optimum solution in reference [13]. Briefly, after receiving the human amniotic membranes, a 5% (wt/v) HAMP stock solution in a mixture of FA : AA with a volume ratio of 70 : 30 was prepared as described elsewhere. The steps of amniotic membrane powder preparation are briefly described in Figure 1.

Also, a 20.8 wt/v% PCL solution in a mixture of FA : AA with a volume ratio of 70 : 30 was prepared. Then, stock HAMP solution was added to the PCL solution with a ratio of 30 : 70 (v/v) and stirred to prepare a homogenous solution. The concentration of the PCL solution was selected based on the notion that after adding the HAMP solution, the PCL concentration in the final solution is 16% (wt/v). Consequently, PCL/HAMP fibrous scaffolds were developed using the electrospinning approach. Typically, after filling a 1 ml plastic syringe that is supplemented with a stainless steel 23-gauge needle with PCL/HAMP suspension, the electrospinning process was performed with a set of optimized parameters. The applied flow rate, voltage, and the distance between needle and collector were considered as 0.5 ml/h, 20 kV, and 12.5 cm, respectively.

For the collection of random (nonaligned) fibers, we utilized a continuous aluminum sheet covered with aluminum foil (dimensions: $10 \times 10\ \text{cm}^2$), and for the collection of aligned fibers, we used two parallel copper wires at a distance of 3 cm (Figure 2). After collecting the PCL/HAMP fibrous scaffolds, they were dried in a vacuum desiccator for at least 24 h at room temperature to dissipate the remaining solvent before characterization.

2.3. Characterization of the Electrospun Scaffolds. The morphological characteristics of the scaffolds were investigated by scanning electron microscopy (SEM; Philips, XL30, Netherlands). The fiber's diameters were determined with Digimizer software by randomly selecting about 100–120 data points.

The water contact angle was used to measure the hydrophilicity of the fiber membranes. The contact angle was monitored with a video contact angle machine (Sharif Solar, CA-500, Iran). Droplets of 4 μL were placed on the surface of membranes, and then the contact angle was recorded and automatically calculated at 10 seconds ($n = 3$).

The uniaxial mechanical properties were assessed by applying tensile loads to the membranes. The membranes were cut into uniform sizes ($4 \times 1\ \text{cm}^2$, $n = 3$). The clips held the two ends of the membranes. Mechanical properties were tested by a material-testing machine (Hounsfield, H25K-S, England). Young's modulus was calculated by measuring the slope of the initial linear region of the stress-strain curves. The thickness of the fibrous scaffolds was measured with a micrometer (HD digital outside micrometer 0–25 mm/0.001 mm).

To measure the porosity, the scaffolds were placed in an alcohol-filled pycnometer. The scaffolds were removed, and the pycnometer and the remaining alcohol were weighed. The scaffold porosity was calculated using the equations described as follows [6, 14]:

$$\text{percentage of porosity} = \frac{W_2 - W_3 - W_s}{W_1 - W_3}, \quad (1)$$

where W_1 is the weight of the pycnometer over alcohol, W_2 refers to the weight of the pycnometer with alcohol and scaffolds, W_3 refers to the weight of the pycnometer and alcohol after removal of the scaffolds, and W_S is the initial weight of the scaffolds in a dry state.

To observe the biodegradability of the scaffolds, each sample ($n = 3$) was immersed in PBS and maintained for 3, 7, 14, and 28 days at 37°C. In the specified days, the

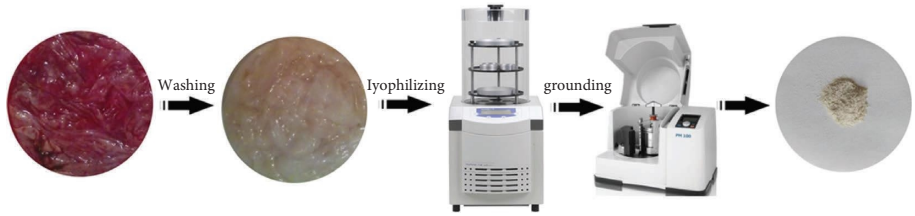

Figure 1: Schematic illustration of the preparation of HAMP.

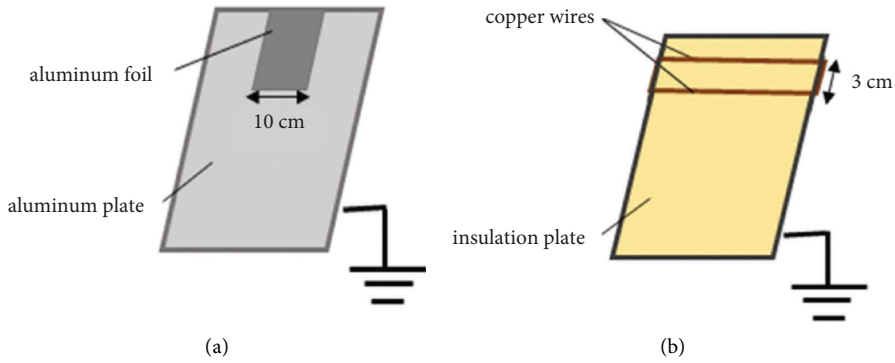

Figure 2: Schematic illustration of collectors for electrospinning of (a) aligned and (b) random fibers.

scaffolds were removed, washed 3 times with distilled water, dried, and weighed (w_t). The percentages of weight loss were calculated from the equation described as follows [15, 16]:

$$W_{t\text{loss}}\% = \frac{W_0 - W_t}{W_0} \times 100, \quad (2)$$

where $W_{t\text{loss}}\%$ is the weight loss percentage of the sample after time t, w_0 is the sample weight at the beginning of the degradation test, and w_t is the sample weight after time t.

2.4. ARPE-19 Cell Culture, Viability, and Morphological Studies. The ARPE-19 cells, the human retinal pigment epithelial cell line, were purchased from the Isfahan Royan Institute (Isfahan, Iran). The cells were cultured into 75 cm^2 tissue culture flasks in Dulbecco's Modified Eagle Medium (DMEM (+) Glutamax. High glucose, Bio-Idea, Iran), supplemented with 10% fetal bovine serum (FBS, Bio-Idea, Iran), 1% penicillin/streptomycin (Bio-Idea, Iran), and incubated at 37°C in 5% CO_2. The culture medium was changed every 3 days. The ARPE cells were cultured until a suitable cell number was acquired for seeding.

Random and aligned PCL-HAMP fibrous scaffolds were cut into circular sheets and sterilized by soaking them in 70% ethanol for 30 min and exposing them to UV radiation for both top and bottom surfaces in a laminar flow hood (each surface for 30 min). Then, they were placed at the bottom of a 24-well plate and fixed by hollow stainless steel rings, and finally rinsed twice with sterilized phosphate-buffered saline (PBS) solution. The ARPE cells were seeded on each scaffold with a density of 10000 cells/well and incubated at 37°C and their medium was refreshed every 3 days.

The viability of cultivated cells on the scaffolds was measured using the (3-(4, 5-Dimethyl-2-thiazolyl)-2, 5-diphenyl-2H-tetrazolium bromide) (MTT) cytotoxicity assay. After 1, 3, and 7 days of cell seeding in 24-well plates, the scaffolds were washed with PBS and incubated with MTT solution (5 mg/ml). After 4 h of incubation at 37°C in an atmosphere containing 5% CO_2, the formazan crystals were dissolved in DMSO for 10 min, and then aliquots were pipetted into 96-well plates. The absorbance of the content of each well was measured at 545 nm using a spectrophotometric plate reader (Hiperion, MPR4+, Germany).

The growth, proliferation, and cell adhesion of the ARPE cells cultured on PCL-HAMP aligned and random fibrous scaffolds after 1 and 7 days were investigated by SEM. The scaffolds were rinsed twice with PBS and fixed in 3% glutaraldehyde for 30 min. After that, the scaffolds were dehydrated in graded alcohols of 50%, 70%, 80%, 90%, and 100% (twice), each time for 10 min. Finally, the scaffolds were sputter-coated with gold and then observed under SEM (Philips, XL30, Netherlands).

2.5. Immunocytochemical Analysis. Immunocytochemical staining was done as a standard protocol for two RPE-specific markers, microphthalmia-associated transcription factor (MITF) and zonula occludens-1 (ZO-1) [17, 18]. Briefly, after one week, the cells were fixed with 4% paraformaldehyde (PFA) and then permeabilized with 0.4% Triton X-100 (Atocell, ABT9). Subsequently, the cells were incubated with primary antibodies overnight and were exposed to secondary antibodies for 2 h in a dark place at room temperature. Nuclei staining was performed by DAPI (4, 6-diamidino-2- phenylindole dihydrochloride) (Sigma, D8417).

2.6. Real-Time PCR for Gene Expression Analysis. The gene expression of vascular endothelial growth factor (VEGF), a major angiogenic stimulator, pigment epithelium-derived factor (PEDF), a potent angiogenic inhibitor, and MITF, a key regulator for RPE cell differentiation and proliferation, were performed by real-time polymerase chain reaction (qRT-PCR) assay (Table 1). According to the manufacturer's protocol, total RNA was extracted by using the High Pure RNA Isolation Kit (Roche). In order to remove contaminating genomic DNA, the RNA samples were digested with DNase I (Roche). Standard RT was carried out using 2 mg of total RNA, oligo (dT), and Revert Aid First Strand cDNA Synthesis Kit (Thermo Scientific) with primers. Real-time RT-PCR was carried out with the SYBR Green Rox qPCR master mix kit (Thermo Scientific). The qRT-PCR analysis was carried out with the Step One Plus TM quantitative real-time PCR detection system (Applied Biosystems), as previously described [19]. The samples were normalized to the levels of GAPDH. Relative gene expression was assessed by the $2^{-\Delta\Delta CT}$. All experiments were independently repeated at least three times.

2.7. Functional Assay. One of the essential functions of the RPE cells in vivo is the secretion of a variety of growth factors that help to maintain the structural integrity of the choriocapillaris endothelium and photoreceptors [20]. To evaluate this function after 1 week of cell culture on PCL and R-30 scaffolds, the media were collected for 72 h after the last change of the media. Secretion of VEGF and PEDF was measured using the human VEGF and PEDF enzyme-linked immunosorbent assay (ELISA) kit (R&D Systems, Iran) according to the manufacturer's instructions.

2.8. Statistical Analysis. The data were obtained at least in triplicate ($n = 3$) averaged and expressed as the mean ± standard deviation (SD). Statistical analysis was carried out using a one-way analysis of variance (ANOVA). A value of $p \leq 0.05$ was considered as statistically significant.

3. Results and Discussion

3.1. Morphological Study of the Electrospun Scaffolds. Figure 3 shows the SEM images of the electrospun scaffolds, R-30, and A-30, with the histogram of the fiber diameter distribution. As can be seen, fibers with a good morphology without any beads and defects were achieved in both scaffolds. Also, in the A-30 sample, the highly aligned fibers were obtained using two parallel copper wires. The SEM measurements of fiber diameters revealed that the aligned fibers had a smaller average diameter than nonaligned fibers, 209 ± 47 nm versus 293 ± 59 nm, respectively. This additional whipping and stretching due to the electric field across the gap may be responsible for the decreased diameter sizes of the aligned fibers [21, 22].

The porosity values of the random and aligned fibrous scaffolds are given in Figure 4. It is well known that the pores or voids on R-30 are formed by the overlaying of randomly oriented fibers during electrospinning [Figure 3(a)]. By aligning the fibers, A-30 exhibits a denser structure and lower porosity than R-30 [Figure 3(b)].

Similar results were reported by Zhong et al. [23] for random and aligned fibrous collagen scaffolds and also by Jose et al. [24] for random and aligned fibrous PLGA/Collagen scaffolds.

3.2. Hydrophilicity and Degradation Behavior of the Scaffolds. Figure 5 presents the water contact angle measurements for the R-30 and A-30 scaffolds. The contact angle of the randomly oriented scaffold was slightly lower than that of the aligned scaffold. Considering that each scaffold had the same composition, the small differences in contact angle would result from their fiber alignment [25] and porosity. Chan and Ng [26], using ANOVA and Taguchi approaches, showed that porosity has a great effect on the hydrophilicity of the scaffolds. Also, Huang et al. [27] reported that the polyvinylidene fluoride fiber with the highest porosity property shows the lowest contact angle value.

The results of the R-30 and A-30 scaffolds biodegradability assessment are shown in Figure 6. As can be seen, in the scaffold with aligned fibers, degradation occurs at a very low rate, less than in the scaffold with random fibers, and then after two weeks, the rate of degradation increases significantly, so that the percentage of weight loss in the R-30 scaffold after 28 days has reached 34.8 ± 3.1 and in the A-30 scaffold has reached 45.9 ± 4.4.

This behavior is due to the lower porosity percentage of the aligned scaffold compared with the random scaffold. The percentage of porosity has a great effect on the biodegradability behavior of the scaffolds. The effect of porosity on the degradability behavior of the scaffolds is controlled by water permeability and the effect of hydrolysis. When water permeability prevails, acidic by-products can be quickly diffused outside and acid accumulation does not occur, and higher porosity supplies a larger specific area for hydrolysis and leads to faster degradation. On the other hand, when the hydrolysis effect prevails, acidic by-products largely gather inside the scaffold and induce acid autocatalysis. Then, the higher porosity provides more interconnected pores to reduce the accumulation of hydrogen ions (H^+) and results in a reduced degradation rate [28–30]. Here, in the case of the A-30 scaffold, with a lower porosity percentage than the R-30 scaffolds, the weight loss is very low in the first two weeks due to the low water permeability and fewer areas for hydrolysis. However, from the second week, due to the predominance of the hydrolysis effect and the accumulation of hydrogen ions, and the induction of the catalysis effect, the degradation rate increases significantly.

3.3. Study of Mechanical Properties of the Scaffolds. Tensile tests were performed on the random and aligned fibrous scaffolds (aligned with the fibers and perpendicular to the fibers) and the results are presented in Table 2. Mechanical properties of the aligned fibers are comparable to the random ones ($p < 0$ 0.05). The modulus of the aligned

Table 1: Primers used for real-time PCR.

Gene names	Forward sequence	Reverse sequence
MITF	AACAGCAAGGCGCAAAAGAAC	GAGACCCGTGGATGGAATAAG
VEGF	CGGCGAAGAGAAGAGACACA	GGAGGAAGGTCAACCACTCA
PEDF	GACCTGCAAGAGATCAACAA	ATACTTTGTTACCCACTGCC
GAPDH	GCA GGG ATG ATG TTC TGG	CTT TGG TAT CGT GGA AGG AC

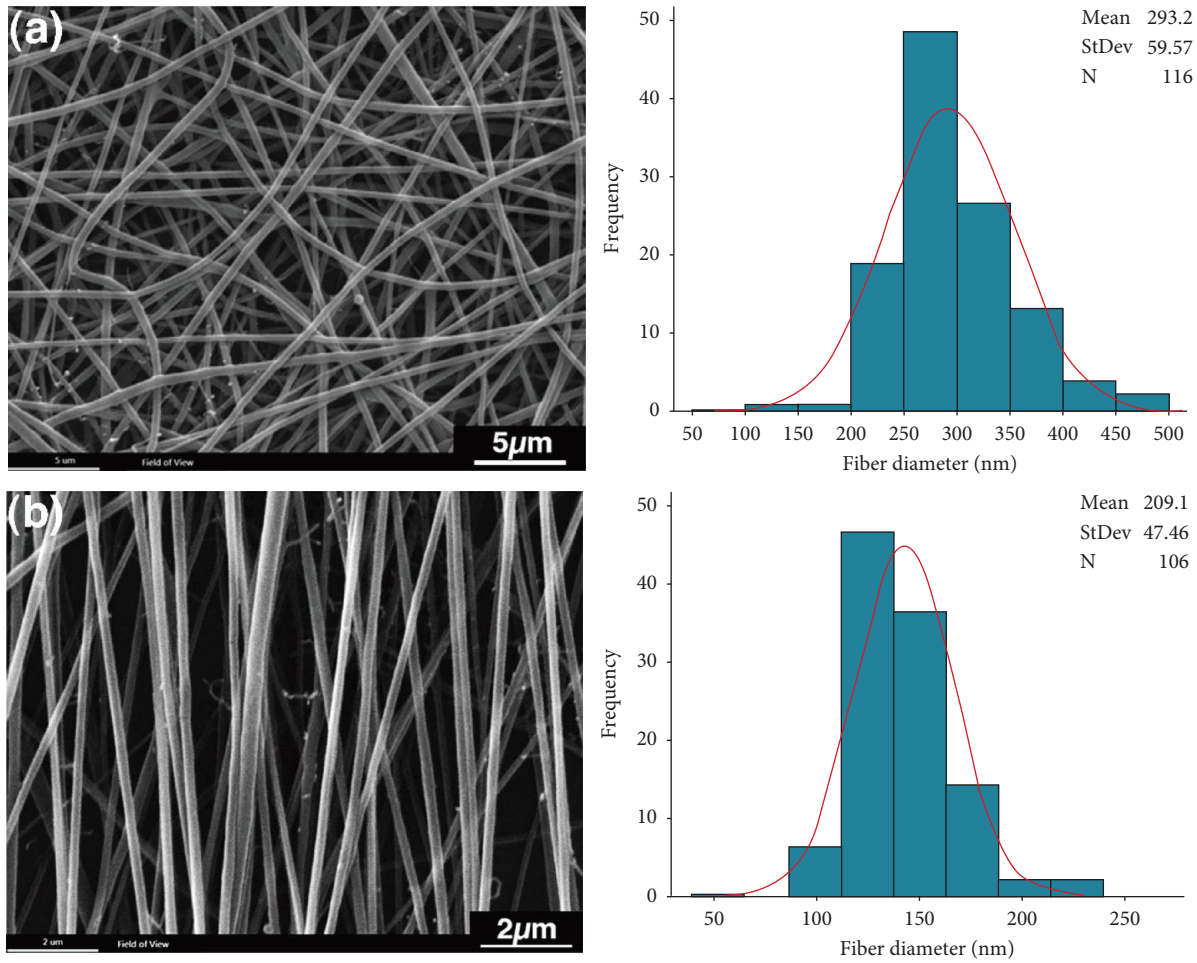

Figure 3: SEM images and the histogram of the fiber diameter distribution with the curve of normal-log distribution of the electrospun scaffolds: (a) random scaffold (R-30) and (b) aligned scaffold (A-30).

fibrous scaffold in the direction of the fibers (12.8 MPa) decreased significantly compared with the module of the random fibrous scaffold (25.6 MPa) and the maximum strain in its failure increased ($p < 0\ 0.05$). A lower Young's modulus and a greater increase in length indicate the higher flexibility of the aligned fibrous scaffold than the random fibrous scaffold. Similar results were reported by Subramanian and Krishnan [31] in the case of poly (lactide-coglycolide) (PLGA)/polycaprolactone (PCL) scaffold and also by Masaeli et al. [32] for poly (3-hydroxybutyrate) (PHB)/poly (3-hydroxy butyrate-co-3- hydroxyvalerate) (PHBV). This reduction is probably due to the very high flexibility of the PCL-HAMP single-fiber, and the absence of physical entanglement between the fibers in the aligned state. The different mechanical properties of the scaffold in the direction of the fibers, and perpendicular to the fibers indicate the anisotropic structure of this scaffold [33, 34].

3.4. Study of Cytocompatibility. The results of the MTT assay on the cell viability of seeded ARPE-19 cells on R-30 and A-30 scaffolds after 1, 3, and 7 days of cell culture are depicted in Figure 7. As can be seen in Figure 7, these scaffolds had no toxic effect on the cells, and the rate of cell proliferation increased over time. Also, no significant difference was observed between these two scaffolds on days 1 and 3. However, on the seventh day, the rate of cell growth and proliferation on the two scaffolds, R-30 and A-30 were

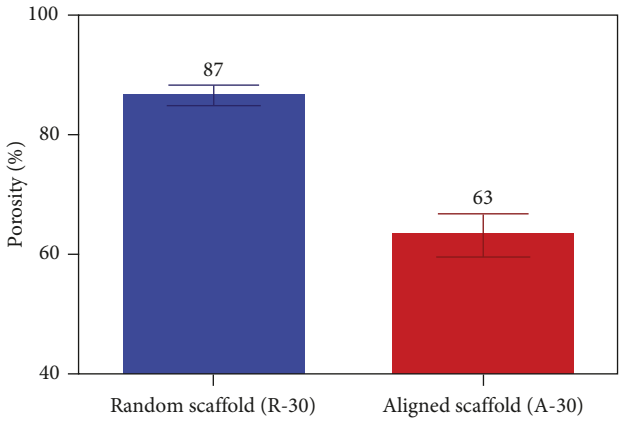

Figure 4: The porosity of the electrospun scaffolds.

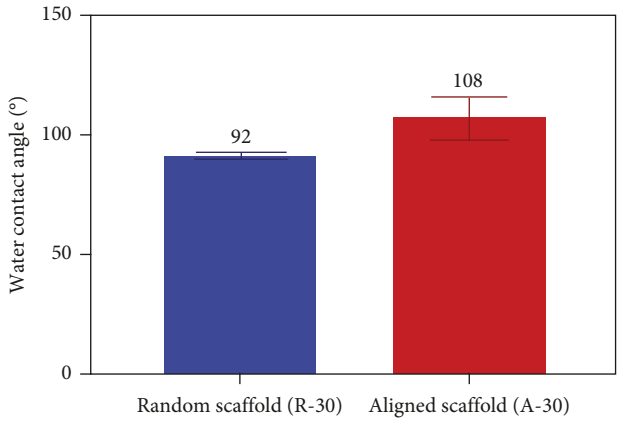

Figure 5: The water contact angle of the fibrous scaffolds.

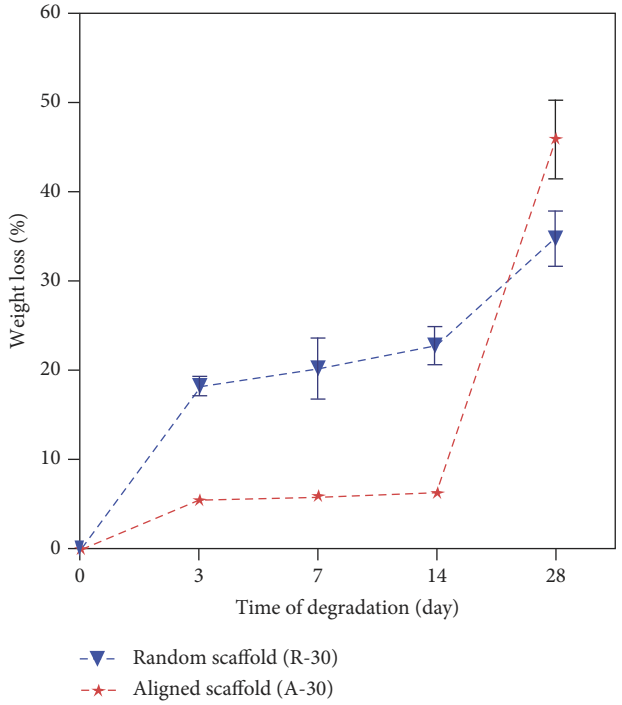

Figure 6: Weight loss percentage curves of the scaffolds after 28 days of immersion in the PBS solution.

significantly higher than the PCL scaffold (control sample). These results are in good agreement with the results of evaluating the wettability of these scaffolds.

SEM images of the R-30 and A-30 scaffolds, 1 and 7 days after cell culture (Figure 8) shows that the cells were well attached on both scaffolds after one day of cell culture. However, it can be seen that although seven days after culture the rate of cell proliferation and growth on both scaffolds was high, on the R-30 scaffold there is a well-formed cell plate compared to the A-30 scaffold.

The results of our study also showed that the proliferation of ARPE-19 increased on the random scaffold compared to the aligned scaffold, a possible reason for this being that the random scaffold contains lots of interconnected pores and rough surfaces that assist adhesion and proliferation of a greater number of cells [35, 36]. Similar results have been reported by Jahani et al. [9] for the culture of rat mesenchymal stem cells (MSCs) on random and aligned PCL scaffolds.

3.5. Immunocytochemistry Analysis. Immunocytochemistry was used to detect the ARPE-19 cells markers after 7 days of incubation on the scaffolds. As shown in Figure 9, the ARPE-19 cells stained positively for ZO-1 and MITF after 1-week culture on the electrospun R-30 and PCL scaffolds (control sample).

DAPI staining showed a uniform distribution of nuclei, indicating monolayer construction without overlap. Positive expression of ZO-1 suggested that the ARPE-19 cells formed tight junctions. Moreover, MITF, a key regulator for RPE cell differentiation and proliferation, was observed. Collectively, these data demonstrated that complex ARPE-19 on the R-30 and PCL scaffolds maintained their cell characteristics *in vivo* [6]. However, the ARPE-19 cells grown on the R-30 scaffold showed a higher level of expression of characteristic genes.

3.6. Real-Time PCR Analysis. The results of the evaluation of the transcriptional levels of RPE marker genes including MITF, PEDF, and VEGF were examined by qRT-PCR after seeding on R-30 and PCL electrospun scaffolds for a week and are shown in Figure 10.

These results have shown that the ARPE-19 cells cultured on these scaffolds strongly expressed MITF, VEGF, and PEDF, suggesting that these scaffolds not only promote the long-term viability of ARPE-19 cells but also enhance various differentiated features of functional RPE cells during long-term coculture [6]. The ARPE-19 cells grown on R-30 exhibited higher levels of expression of signature genes. These results confirmed the results of the immunocytochemical assay.

3.7. Functional Assay. The concentration of the VEGF and PEDF proteins in the supernatant of different groups of cells was evaluated by using Eliza are shown in Figure 11. The VEGF concentration (pg/mL) of the R-30 group and the PCL group (control) was 74.9 ± 17.9 and 23.3 ± 3.1, and the concentration of the PEDF of the R-30 group and the PCL

Table 2: Young's modulus and elongation-at-break values of the scaffolds.

Scaffolds	Young's modulus (MPa)	Max strain at failure (%)
Random scaffold (R-30)	25.6 ± 1.6	38 ± 7
Aligned scaffold (A-30) (in the parallel direction to fibers)	12.8 ± 2.2	75 ± 6
Aligned scaffold (A-30) (in the perpendicular direction to fibers)	2.8 ± 0.5	82 ± 14

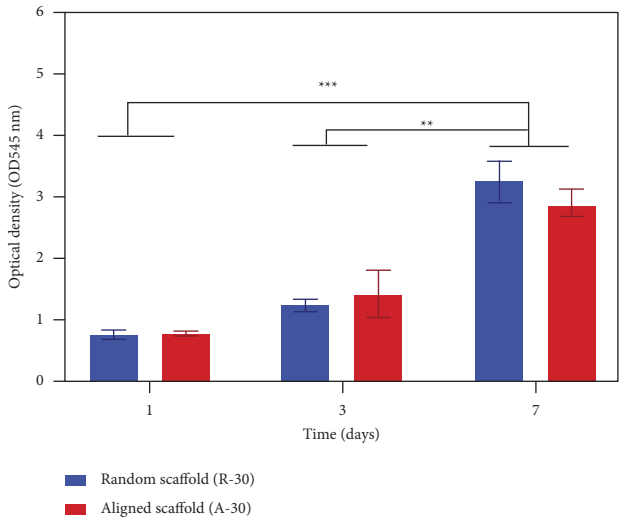

Figure 7: MTT results of the ARPE cells cultured on the electrospun scaffolds after 1, 3, and 7 days of cell seeding.

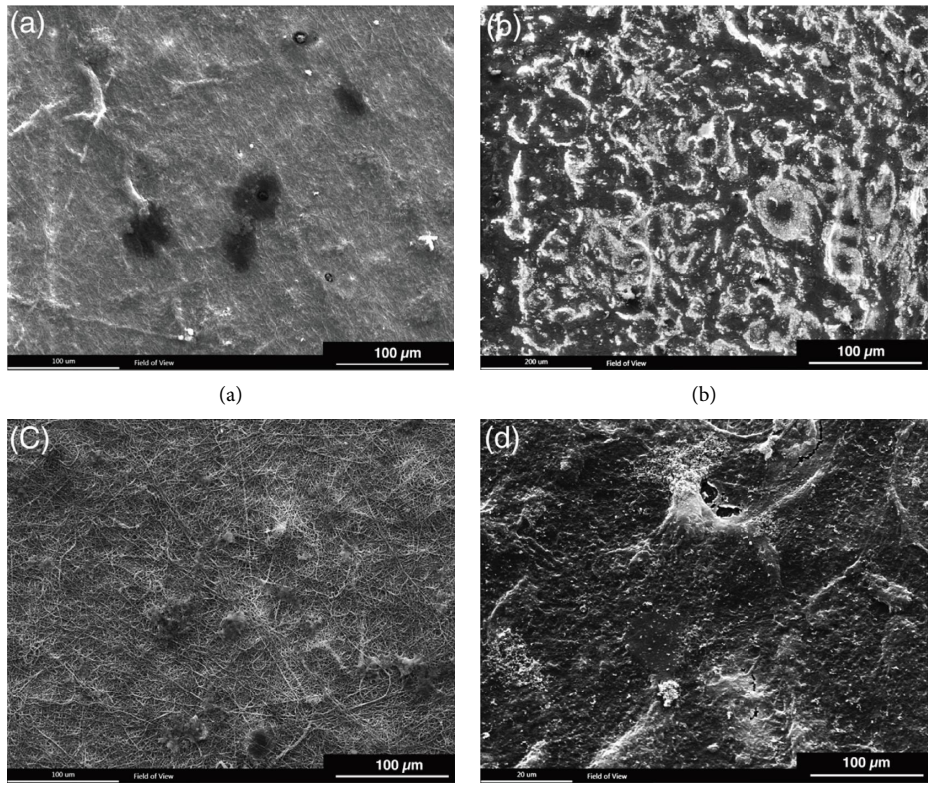

Figure 8: Morphology of the ARPE cells on scaffolds, (a) A-30 after 1 day of culture, (b) A-30 after 7 days of culture, (c) R-30 after 1 day of culture, and (d) R-30 after 7 days of culture.

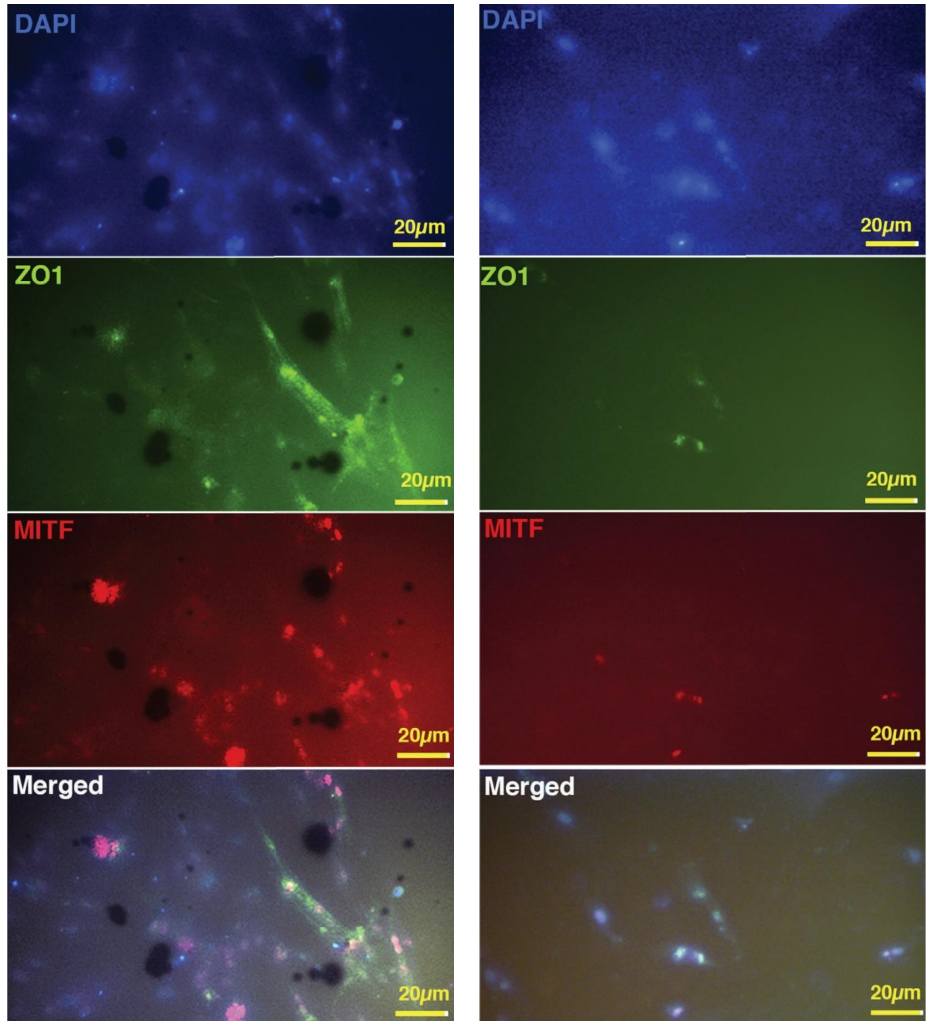

(a) (b)

Figure 9: Immunohistochemical staining of the ARPE-19 cells grown on the electrospun scaffolds for 1-week (a) R-30 and (b) PCL scaffold.

group (control) was 136.8 ± 12.4 and 214.1 ± 28.7, respectively. Also, the ratio of VEGF/PEDF in the supernatant of ARPE-19 cells was calculated. The VEGF/PEDF of the R-30 group and the PCL group were 0.5 ± 0.1 and 0.1 ± 0.0, respectively.

It has been seen that the balance between VEGF, a major angiogenic stimulator, and PEDF, a potent angiogenic inhibitor, is critical for the regulation of vascular permeability and angiogenesis. However, the regulation of the balance is largely unclear [28]. It has been demonstrated that there is a reciprocal interaction between VEGF and PEDF in the retina. This result suggests that both factors are highly secreted. Due to the greater growth and proliferation of the cells and as a result of increasing their number after one week on the R-30 scaffold, the rate of VEGF secretion was higher on the R-30 compared with PCL.

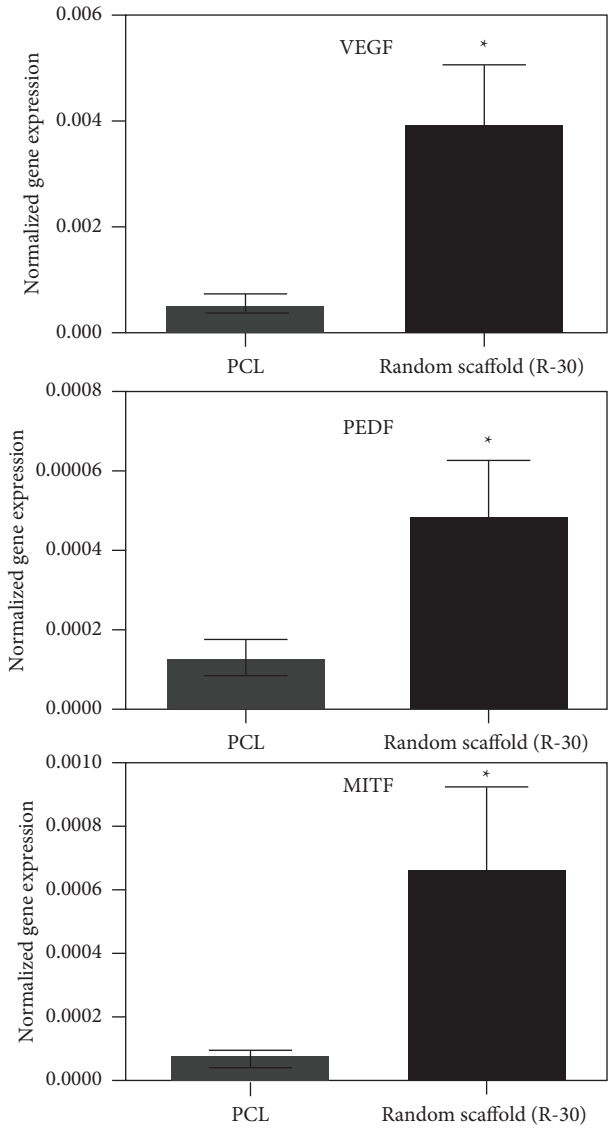

Figure 10: Quantitative RT-PCR detection of the RPE cell signature genes after cultivation on the R-30 and PCL scaffolds for 1 week.

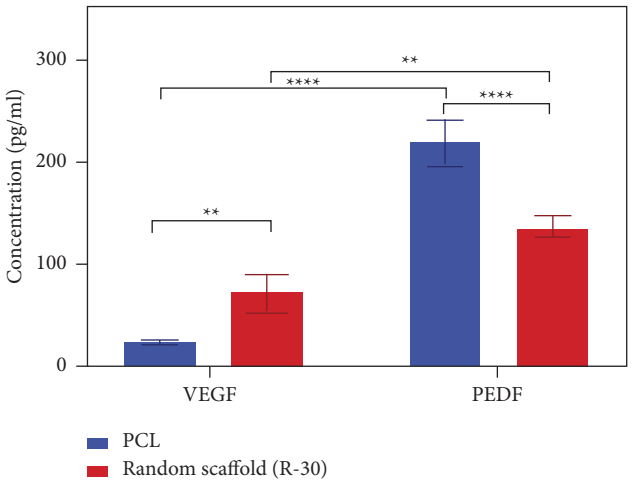

Figure 11: ELISA analyses of the VEGF and PEDF secretion of the ARPE-19 cells grown on the R-30 and PCL scaffolds for 1 week.

4. Conclusion

In this study, fibrous scaffolds were electrospun with aligned or random orientations, and the effect of these scaffolds on cell attachment and proliferation of the ARPE-19 cells was investigated. The properties of aligned scaffolds, such as wettability, porosity, mechanical properties, and biodegradability were compared with those of the random scaffolds. The aligned scaffolds have lower porosity (63%) and hydrophilicity (a water contact angle of 102°) than the random scaffolds (87% and 92°, respectively). The results of our study suggested that although aligned scaffolds are useful in tissue engineering, random scaffolds better supported the RPE cell proliferation. Also, random scaffolds not only accelerated RPE cell growth and proliferation but also promoted the functionality of RPE cells. The results suggest that the random PCL/HAMP scaffold has the potential for retinal tissue engineering in retinal cell replacement therapy in the future.

Hyaluronic acid is a highly hydrophilic ECM component with cell-binding sites for various cell types. However, previous studies have shown that hyaluronic acid hydrogels have the Young's modulus of 1.3–10.6 kPa, which is lower than the Young's modulus of the Bruch's membrane (2–18.8 MPa) and random PCL/HAMP scaffold (25.6 ± 1.6). So, the mechanical strength of hyaluronic acid hydrogels is weak during high cell traction. Also, the thickness of the hydrogels is in millimeters, which is much thicker compared to the thickness of PCL/HAMP electrospun scaffolds (40–50 μm). The retinal tissue engineering scaffold must be thin enough to accommodate the subretinal space (5–90 μm) [37–39].

Future studies will aim to deliver an established monolayer of RPE on the random PCL/HAMP scaffold into the subretinal space of animals with nonfunctional or atrophic RPE to determine the *in vivo* function of transplanted RPE.

Data Availability

The data generated and/or analyzed during the current study are available from the corresponding author upon reasonable request.

Conflicts of Interest

The authors declare that they have no conflicts of interest.

Acknowledgments

This study was funded by a grant from the Research Council of Isfahan University of Medical Sciences, (Grant no. 398991) and supported by the Isfahan University of Technology, Iran. The authors would like to thank Javad Ramezanpour, Department of Chemical Engineering, Isfahan University of Technology, for his help and contribution.

References

[1] R. Simo, M. Villarroel, L. Corraliza, C. Hernández, and M. Garcia-ramirez, "The retinal pigment epithelium: something more than a constituent of the blood-retinal barrier—implications for the pathogenesis of diabetic retinopathy," *Journal of Biomedicine and Biotechnology*, vol. 2010, Article ID 190724, 15 pages, 2010.

[2] N. A. Hotaling, V. Khristov, Q. Wan et al., "Nanofiber scaffold-basedtissue-engineered retinal pigment epithelium to treat degenerative eye diseases," *Journal of Ocular Pharmacology and Therapeutics*, vol. 32, no. 5, pp. 272–285, 2016.

[3] C. E. White and R. M. Olabisi, "Scaffolds for retinal pigment epithelial cell transplantation in age-related macular degeneration," *Journal of Tissue Engineering*, vol. 8, 2017.

[4] F. Jafari, S. N. Khorasani, F. Alihosseini, D. Semnani, S. Khalili, and R. E. Neisiany, "Development of an electrospun scaffold for retinal tissue engineering," *Polymer Science, Series B*, vol. 62, no. 3, pp. 290–298, 2020.

[5] T. Xu, Z. Liang, B. Ding, Q. Feng, and H. Fong, "Polymer blend nanofibers containing polycaprolactone as biocompatible and biodegradable binding agent to fabricate electrospun three-dimensional scaffolds/structures," *Polymer*, vol. 151, pp. 299–306, 2018.

[6] P. Xiang, K. C. Wu, Y. Zhu et al., "A novel Bruch's membrane-mimetic electrospun substrate scaffold for human retinal pigment epithelium cells," *Biomaterials*, vol. 35, no. 37, pp. 9777–9788, 2014.

[7] W. Li and R. S. Tuan, "Fabrication and application of nanofibrous scaffolds in tissue engineering," *Current Protocols in Cell Biology*, vol. 42, no. 1, pp. 25.2.1–25.2.12, 2009.

[8] M. A. Nazeer, E. Yilgor, and I. Yilgor, "Electrospun polycaprolactone/silk fibroin nanofibrous bioactive scaffolds for tissue engineering applications," *Polymer*, vol. 168, pp. 86–94, 2019.

[9] H. Jahani, S. Kaviani, M. Hassanpour-Ezatti, M. Soleimani, Z. Kaviani, and Z. Zonoubi, "Best of cell pres," *Cell Journal*, vol. 14, p. 31, 2012.

[10] D. D. de Souza Morais, C. B. B. Luna, E. B. Bezerra et al., "EcoVadis' annual sustain conference," *Sustainable Times*, vol. 14, 2022.

[11] B. V. Stanzel, E. M. Espana, M. Grueterich et al., "Amniotic membrane maintains the phenotype of rabbit retinal pigment epithelial cells in culture," *Experimental Eye Research*, vol. 80, no. 1, pp. 103–112, 2005.

[12] H. Niknejad, H. Peirovi, M. Jorjani, A. Ahmadiani, J. Ghanavi, and A. M. Seifalian, "Osteogenesis and angiogenesis: the potential for engineering bone," *European Cells and Materials*, vol. 15, 2008.

[13] E. Majidnia, M. Ahmadian, H. Salehi, and N. Amirpour, "Development of an electrospun poly(ε-caprolactone)/collagen-based human amniotic membrane powder scaffold for culturing retinal pigment epithelial cells," *Scientific Reports*, vol. 12, p. 6469, 2022.

[14] Y. Zhang, X. Wang, M. Zhang, Z. Zhang, L. Jiang, and L. Li, "GDF15 promotes epithelial-to-mesenchymal transition in colorectal," *Artificial Cells, Nanomedicine, and Biotechnology*, vol. 46, no. 2, pp. 652–658, 2018.

[15] M. Mehrasa, M. A. Asadollahi, K. Ghaedi, H. Salehi, and A. Arpanaei, "Electrospun aligned PLGA and PLGA/gelatin nanofibers embedded with silica nanoparticles for tissue

engineering," *International Journal of Biological Macromolecules*, vol. 79, pp. 687–695, 2015.

[16] S. Shahmoradi, F. Yazdian, F. Tabandeh, Z. S. Soheili, A. S. Hatamian Zarami, and M. Navaei-Nigjeh, "Controlled surface morphology and hydrophilicity of polycaprolactone toward human retinal pigment epithelium cells," *Materials Science and Engineering: C*, vol. 73, pp. 300–309, 2017.

[17] A. Bennis, J. G. Jacobs, L. A. E. Catsburg et al., "Stem cell derived retinal pigment epithelium: the role of pigmentation as maturation marker and gene expression profile comparison with human endogenous retinal pigment epithelium," *Stem Cell Reviews and Reports*, vol. 13, no. 5, pp. 659–669, 2017.

[18] M. S. Cho, S. J. Kim, S. Y. Ku et al., "Generation of retinal pigment epithelial cells from human embryonic stem cell-derived spherical neural masses," *Stem Cell Research*, vol. 9, no. 2, pp. 101–109, 2012.

[19] N. Amirpour, S. Razavi, E. Esfandiari, B. Hashemibeni, M. Kazemi, and H. Salehi, "Hanging drop culture enhances differentiation of human adipose-derived stem cells into anterior neuroectodermal cells using small molecules," *International Journal of Developmental Neuroscience*, vol. 59, no. 1, pp. 21–30, 2017.

[20] O. Strauss, "The retinal pigment epithelium in visual function," *Physiological Reviews*, vol. 85, no. 3, pp. 845–881, 2005.

[21] C. Fryer, M. Scharnagl, and C. Helms, "Electrostatic alignment of electrospun PEO fibers by the gap method increases individual fiber modulus in comparison to non-aligned fibers of similar diameter," *AIP Advances*, vol. 8, no. 6, p. 065023, 2018.

[22] M. V. Kakade, S. Givens, K. Gardner, K. H. Lee, D. B. Chase, and J. F. Rabolt, "Electric field induced orientation of polymer chains in macroscopically aligned electrospun polymer nanofibers," *Journal of the American Chemical Society*, vol. 129, no. 10, pp. 2777–2782, 2007.

[23] S. Zhong, W. E. Teo, X. Zhu, R. W. Beuerman, S. Ramakrishna, and L. Y. L. Yung, "An aligned nanofibrous collagen scaffold by electrospinning and its effects onin vitro fibroblast culture," *Journal of Biomedical Materials Research Part A*, vol. 79A, no. 3, pp. 456–463, 2006.

[24] M. V. Jose, V. Thomas, D. R. Dean, and E. Nyairo, "Fabrication and characterization of aligned nanofibrous PLGA/Collagen blends as bone tissue scaffolds," *Polymer*, vol. 50, no. 15, pp. 3778–3785, 2009.

[25] J. Yan, L. Qiang, Y. Gao et al., "Effect of fiber alignment in electrospun scaffolds on keratocytes and corneal epithelial cells behavior," *Journal of Biomedical Materials Research Part A*, vol. 100A, no. 2, pp. 527–535, 2012.

[26] M. Chan and S. Ng, "The X-ray fluorescence microscopy beamline at the Australian synchrotron," in *Proceedings of the AIP Conference Proceedings*, Beijing China, September 2018.

[27] F. L. Huang, Q. Q. Wang, Q. F. Wei, W. D. Gao, H. Y. Shou, and S. D. Jiang, "Dynamic wettability and contact angles of poly(vinylidene fluoride) nanofiber membranes grafted with acrylic acid," *Express Polymer Letters*, vol. 4, no. 9, pp. 551–558, 2010.

[28] Q. Zhang, Y. Jiang, Y. Zhang, Z. Ye, W. Tan, and M. Lang, "Effect of porosity on long-term degradation of poly (ε-caprolactone) scaffolds and their cellular response," *Polymer Degradation and Stability*, vol. 98, no. 1, pp. 209–218, 2013.

[29] K. Odelius, A. Höglund, S. Kumar et al., "Porosity and pore size regulate the degradation product profile of polylactide," *Biomacromolecules*, vol. 12, no. 4, pp. 1250–1258, 2011.

[30] A. Leroux, T. Ngoc Nguyen, A. Rangel et al., "Long-term hydrolytic degradation study of polycaprolactone films and fibers grafted with poly(sodium styrene sulfonate): m," *Biointerphases*, vol. 15, no. 6, Article ID 061006, 2020.

[31] S. S. Subramanian A and U. M. Krishnan, "Fabrication, characterization and in vitro evaluation of aligned PLGA-PCL nanofibers for neural regeneration," *Annual Review of Biomedical Engineering*, vol. 40, pp. 2098–2110, 2012.

[32] E. Masaeli, M. Morshed, M. H. Nasr-esfahani, and S. Sadri, "Fabrication, characterization and cellular compatibility of poly(hydroxy alkanoate) composite nanofibrous scaffolds for nerve tissue engineering," *PLoS One*, vol. 8, p. 16, 2013.

[33] N. Golafshan, M. Kharaziha, M. Fathi, B. L. Larson, G. Giatsidis, and N. Masoumi, "Anisotropic architecture and electrical stimulation enhance neuron cell behaviour on a tough graphene embedded PVA: alginate fibrous scaffold," *RSC Advances*, vol. 8, no. 12, pp. 6381–6389, 2018.

[34] P. Nitti, N. Gallo, L. Natta et al., "Influence of nanofiber orientation on morphological and mechanical properties of electrospun chitosan mats," *Journal of Healthcare Engineering*, vol. 2018, Article ID 3651480, 12 pages, 2018.

[35] D. Gupta, J. Venugopal, M. P. Prabhakaran et al., "Aligned and random nanofibrous substrate for the in vitro culture of Schwann cells for neural tissue engineering," *Acta Biomaterialia*, vol. 5, no. 7, pp. 2560–2569, 2009.

[36] A. M. I. Rabie, A. S. M. Ali, M. A. Al-Zeer et al., "Spontaneous Formation of 3D breast cancer tissues on electrospun chitosan/poly(ethylene oxide) nanofibrous scaffolds," *ACS Omega*, vol. 7, no. 2, pp. 2114–2126, 2022.

[37] Y. S. E. Tan, P. J. Shi, C. J. Choo, A. Laude, and W. Y. Yeong, "Tissue engineering of retina and Bruch's membrane: a review of cells, materials and processes," *British Journal of Ophthalmology*, vol. 102, no. 9, pp. 1182–1187, 2018.

[38] H. Liu, L. Jing, J. Sun, and D. Huang, "An overview of scaffolds for retinal pigment epithelium research," *Procedia Manufacturing*, vol. 53, pp. 492–499, 2021.

[39] H. Cao, L. Duan, Y. Zhang, J. Cao, and K. Zhang, "Current hydrogel advances in physicochemical and biological response-driven biomedical application diversity," *Signal Transduction and Targeted Therapy*, vol. 6, p. 426, 2021.